

## Resonant Raman scattering in nanoscale pentacene films

Rui He,<sup>a)</sup> Irene Dujovne,<sup>b)</sup> Liwei Chen, Qian Miao, Cyrus F. Hirjibehedin,<sup>b)</sup> Aron Pinczuk,<sup>b)</sup> and Colin Nuckolls  
*Columbia University, New York, New York 10027*

Christian Kloc

*Bell Labs, Lucent Technologies, Murray Hill, New Jersey 07974*

Arza Ron

*Department of Chemistry, Technion—Israel Institute of Technology, Haifa 32000, Israel*

(Received 30 October 2003; accepted 16 December 2003)

Resonant Raman scattering intensities from nanoscale films of pentacene display large resonant enhancements that enable observation of vibrational modes in monolayer cluster films. The resonant enhancements occur when the outgoing photon energy overlaps the free exciton optical transitions observed in luminescence. The results point to the significant potential of resonant Raman methods in the characterization of nanoscale structures of organic molecular semiconductors. © 2004 American Institute of Physics. [DOI: 10.1063/1.1646756]

Pentacene ( $C_{22}H_{14}$ ) is an organic molecular semiconductor (OMS) of great interest for potential applications in thin-film transistors.<sup>1,2</sup> While pentacene transistors exhibit good carrier mobility,<sup>3–5</sup> the characteristics depend in a crucial way on the structural and electrical perfection of the materials used in the fabrication of the devices. Raman scattering is a flexible high-resolution optical spectroscopy probe of the structural and electronic properties of materials. However, Raman scattering signals from nanoscale films of OMSs with thickness reaching the monolayer dimension ( $\sim 2$  nm) may be too weak to be observable and thus limit the applications of the method. Resonance Raman spectroscopy may enable the observation of signals from nanoscale films.<sup>6,7</sup>

In this letter, we show that resonant enhancements of Raman scattering intensities offer the sensitivity required to study pentacene films of nanoscale thickness. Our films are fabricated on thermally oxidized Si substrates similar to those employed in state-of-the-art devices.<sup>3,4</sup> The penetration depth of light in the present experiments is typically about  $1 \mu\text{m}$ <sup>8,9</sup> which, being comparable to the channel depth of current field-effect transistors based on OMSs,<sup>5,10</sup> makes resonant Raman scattering an ideal probing method to study interfacial effects in molecular organic films and field-effect transistor devices.

Strong resonant enhancement profiles of Raman cross sections are observed in nanoscale multilayer films of less than 100 nm thickness. The peak in resonant enhancement occurs when the outgoing photon energy overlaps the free exciton (FE) optical transitions seen in luminescence. Similar overlap between the energy of the FE and the maximum in resonant enhancement is observed in a pentacene single crystal. The exciton in the nanoscale multilayer films exhibits a significant blueshift ( $\sim 40$  meV) from that in the crystal. This shift may be linked to different polymorphic structures, defects, and grain boundaries in the nanoscale films in comparison to the bulk crystal. Pentacene monolayer clusters in a

discontinuous film exhibit broadened Raman modes and a strong resonant Raman enhancement at outgoing photon energies blueshifted by about 100 meV from that in the crystal. The FE transition is not observed in the luminescence spectrum of this film.

We present results taken at 77 K from two films of average thickness, 65 nm (**F1**) and 1.9 nm (**F2**), and a pentacene single crystal (**CR**). **CR** was prepared by physical vapor transport methods, as discussed in detail by Laudise *et al.*,<sup>11</sup> and the films **F1** and **F2** were prepared by thermal deposition in high vacuum on oxidized silicon substrates kept at 300 K. **F1** was grown with a deposition rate of about 0.5 Å/s, while a deposition rate of 0.1 monolayer/min and a typical run time of 2 min were used to fabricate sample **F2**. Figure 1(a) displays an atomic force microscope (AFM) height image of sample **F1** in which small grains can be seen. The film thickness at different places can vary from 40 to 80 nm. Figure 1(b) is a micrograph of the ultrathin pentacene film **F2** with single-molecular-layer thickness. It shows that the substrate is fractionally covered by island-like monolayer pentacene clusters of 1.9 nm average thickness, which is roughly the length of a single pentacene molecule.<sup>12</sup>

Samples were mounted in a cryostat with windows for optical access and were immersed in liquid nitrogen. Spectra were excited with the linearly polarized emission of a dye

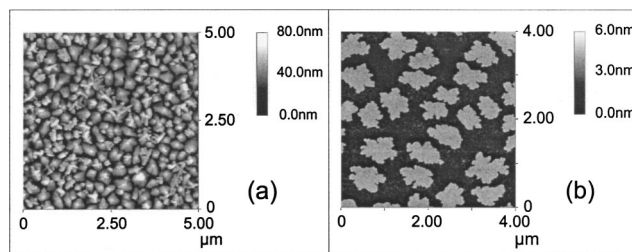


FIG. 1. AFM images of (a) pentacene film with an average thickness of 65 nm (sample **F1**) showing submicron grains. (b) Discontinuous pentacene film of average thickness of 1.9 nm (sample **F2**). The monolayer clusters are relatively large, with lateral dimensions approaching  $1 \mu\text{m}$ . In this panel, the dark color background is the substrate.

<sup>a)</sup>Electronic mail: rh2017@columbia.edu

<sup>b)</sup>Also at: Bell Labs, Lucent Technologies, Murray Hill, New Jersey 07974.

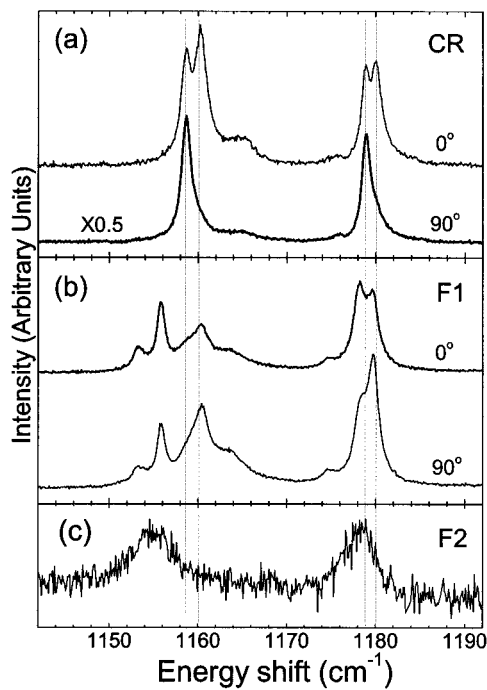


FIG. 2. Raman scattering from C–H in-plane bending modes at 77 K. (a) Sample **CR** at two incident polarizations. The angles were measured with respect to the horizontal plane. Instrument resolution is  $0.33 \text{ cm}^{-1}$ . (b) Sample **F1** at two different incident polarizations. Angles are as in panel (a). Instrument resolution is  $0.4 \text{ cm}^{-1}$ . (c) Sample **F2** with an instrument resolution of  $3.6 \text{ cm}^{-1}$ .

laser tunable over the wavelength range from 5850 to 6850 Å, which overlaps with the range of fundamental optical transitions in pentacene.<sup>9</sup> Incident power density was kept below  $5 \text{ W/cm}^2$ . Scattered light was analyzed by a Spex 1404 double spectrometer with holographic master gratings and CCD multichannel detection.

Pentacene crystals and thin films have numerous Raman active modes.<sup>13,14</sup> We measured intramolecular vibrations and intermolecular lattice modes. The observed low-energy intermolecular lattice modes are in the range of  $35$  to  $100 \text{ cm}^{-1}$ . There are significant energy differences between the lattice modes of **CR** and **F1** samples. These differences are attributed to different polymorphism in the film and in the crystal. Lattice modes are thus instrumental in the structural characterization of pentacene nanoscale films. We focus here on the intramolecular modes in the region of  $1140$ – $1190 \text{ cm}^{-1}$ , where pentacene has strong Raman signals. The vibrational modes in this energy range have been assigned to C–H in-plane bending.<sup>13–15</sup>

Figure 2(a) displays Raman spectra obtained from the crystal **CR**. The relative intensities of the modes at  $1158$  and  $1160 \text{ cm}^{-1}$  and the two modes at  $1179$  and  $1180 \text{ cm}^{-1}$  change with incident polarization due to their different depolarization ratios.<sup>15</sup> Figures 2(b) and 2(c), respectively, show Raman spectra from films **F1** and **F2**. Spectra of sample **F1** show more Raman lines than **CR** in the region of  $1150$ – $1170 \text{ cm}^{-1}$  due to the presence of polymorph phases in the film.<sup>13,15,16</sup> Disorder and inhomogeneity, which break the intrinsic symmetry of the lattice and the molecule in the film, could also contribute to the appearance of additional Raman lines in sample **F1**. The weaker polarization dependence than sample **CR** in **F1** is consistent with the polycrystalline nature

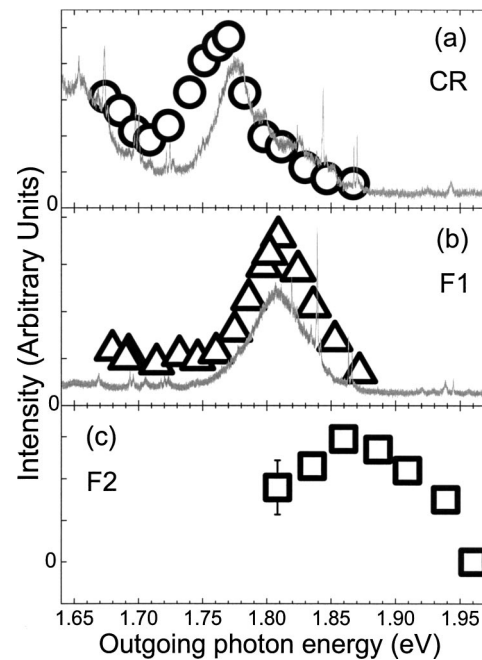


FIG. 3. Profiles of resonant enhancements of Raman scattering intensities by C–H in-plane bending modes are shown as circles, triangles, and squares. Zero Raman intensities are labeled for each panel. Luminescence spectra are shown as continuous traces. All data are at 77 K. (a) Results for the mode at  $1179 \text{ cm}^{-1}$  in sample **CR**. The polarization was fixed at  $90^\circ$ . (b) Results for the mode at  $1178 \text{ cm}^{-1}$  in sample **F1**. The polarization was fixed at  $0^\circ$ . (c) Results for the mode at  $1178 \text{ cm}^{-1}$  in sample **F2**. Luminescence spectrum (not shown) displays no structures in this region. A typical error bar is shown for this sample.

of the film. Peak doublets were not resolved in sample **F2**. The two Raman peaks at  $1155$  and  $1178 \text{ cm}^{-1}$  in **F2** both shift to lower energy and are much broadened compared to similar modes in sample **CR** in this region. Interlayer interactions are absent in this monolayer film, so that the C–H bonds at the end of the molecule away from the  $\text{SiO}_2$ /pentacene interface are in a more relaxed situation than those in the crystal. This relaxation of the C–H bonds may explain the slight redshift of the vibrational energies. The broadening of the Raman lines in **F2** could result from disorder and interactions between pentacene molecules and the substrate. The C–H bonds at the  $\text{SiO}_2$ /pentacene interface have different environments from those at the other end of the molecule, and the amorphous  $\text{SiO}_2$  substrate has a surface corrugation of about  $0.1 \text{ nm}$ , which leads to further inhomogeneity of the environments of C–H bonds.

The continuous traces in Fig. 3 show luminescence from two of the samples in this study. In sample **CR**, the peak at  $1.77 \text{ eV}$  in the luminescence spectrum was assigned to the FE transition band,<sup>17</sup> while the band at lower energy ( $1.65 \text{ eV}$ ) was assigned to the self-trapped exciton band.<sup>17</sup> Figure 3(a) shows that the profile of the Raman intensities of the mode at  $1179 \text{ cm}^{-1}$  has a maximum when the photon energy of the scattered light overlaps the FE transition at  $1.77 \text{ eV}$  (outgoing photon resonance). Within the tunable range of the laser, another resonance is seen when the outgoing photon energy coincides with the self-trapped exciton emission at  $1.65 \text{ eV}$ .

Figure 3(b) shows the profile of outgoing resonance enhancements of Raman scattering intensities of the mode at  $1178 \text{ cm}^{-1}$  in sample **F1**. The luminescence from the sample

reveals that the FE emission band appears at 1.81 eV, blue-shifted by about 40 meV from the FE band of the crystal **CR**. This energy difference could be associated with more structural defects, grain boundaries, and the presence of polymorph phases<sup>16</sup> in the film. The molecular stacking in the polycrystalline and polymorphic thin film is not as perfect as in the crystal.<sup>18</sup> The associated reduction of the molecular orbital overlaps between neighboring molecules in the film<sup>18,19</sup> may shift the exciton transition to higher energy. The peak in the resonant enhancement profile also occurs when the outgoing photon energy overlaps the FE transition.

Figure 3(c) displays the profile of outgoing resonance enhancements of Raman intensities of the mode at 1178  $\text{cm}^{-1}$  in sample **F2**. A well-defined outgoing resonance is detected, while the FE emission band is not resolved in the luminescence spectrum. The position of the outgoing resonance (1.86 eV) is 50 meV higher than that in sample **F1** and 90 meV higher than that in **CR**. It is conceivable that this outgoing resonance is linked to a strictly two-dimensional exciton that becomes the FE in thicker nanoscale films. In this scenario, the significant blueshift of 50 meV from the thicker nanoscale film **F1** may result from the confinement of excitons within the layer that prevents motion in the direction perpendicular to the substrate surface.

In summary, strong outgoing resonances of Raman scattering intensities of C–H bending modes are observed in nanoscale pentacene films. The enhancements enable the observation of ultrathin layers that reach down to monolayer thickness. The maximum resonance enhancement occurs when outgoing photon energies overlap the free exciton luminescence. These excitations exhibit blueshifts when going from bulk crystal to nanoscale films and to monolayer discontinuous films. In the monolayer film, the confinement effect could contribute to the blueshift. These results demonstrate the potential of resonant Raman scattering as an optical probe for the study of devices, multilayers, and interfaces of organic molecular semiconductors.

This work was supported in part by the Nanoscale Science and Engineering Initiative of the National Science Foundation under NSF Award Number CHE-0117752 and by a research grant of the W. M. Keck Foundation. One of the authors (L.C.) thanks A. Schrott for help with sample preparation at the IBM T. J. Watson Research Center.

- <sup>1</sup>H. Klauk, D. J. Gundlach, J. A. Nichols, and T. N. Jackson, *IEEE Trans. Electron Devices* **46**, 1258 (1999).
- <sup>2</sup>H. Klauk, D. J. Gundlach, and T. N. Jackson, *IEEE Electron Device Lett.* **20**, 289 (1999).
- <sup>3</sup>D. J. Gundlach, Y. Y. Lin, T. N. Jackson, S. F. Nelson, and D. G. Schlom, *IEEE Electron Device Lett.* **18**, 87 (1997).
- <sup>4</sup>S. F. Nelson, Y.-Y. Lin, D. J. Gundlach, and T. N. Jackson, *Appl. Phys. Lett.* **72**, 1854 (1998).
- <sup>5</sup>V. Y. Butko, X. Chi, D. V. Lang, and A. P. Ramirez, *Appl. Phys. Lett.* **83**, 4773 (2003).
- <sup>6</sup>M. Cai, M. D. Mowery, J. E. Pemberton, and C. E. Evans, *Appl. Spectrosc.* **54**, 31 (2000).
- <sup>7</sup>I. R. J. Lyall and D. N. Batchelder, *Br. Polym. J.* **17**, 372 (1985).
- <sup>8</sup>J. Puigdollers, C. Voz, A. Orpella, I. Martin, M. Vetter, and R. Alcubilla, *Thin Solid Films* **427**, 367 (2003).
- <sup>9</sup>S. P. Park, S. S. Kim, J. H. Kim, C. N. Whang, and S. Im, *Appl. Phys. Lett.* **80**, 2872 (2002).
- <sup>10</sup>A. Ramirez (private communication).
- <sup>11</sup>R. A. Laudise, C. Kloc, P. G. Simpkins, and T. Siegrist, *J. Cryst. Growth* **187**, 449 (1998).
- <sup>12</sup>R. Ruiz, B. Nickel, N. Koch, L. C. Feldman, R. F. Haglund, Jr., A. Kahn, F. Family, and G. Scoles, *Phys. Rev. Lett.* **91**, 136102 (2003).
- <sup>13</sup>A. Brillante, R. G. Della Valle, L. Farina, A. Girlando, M. Masino, and E. Venuti, *Chem. Phys. Lett.* **357**, 32 (2002).
- <sup>14</sup>L. Colangeli, V. Mennella, G. A. Baratta, E. Bussoletti, and G. Strazzulla, *Astrophys. J.* **396**, 369 (1992).
- <sup>15</sup>T. Jentzsch, H. J. Juepner, K.-W. Brzezinka, and A. Lau, *Thin Solid Films* **315**, 273 (1998).
- <sup>16</sup>C. C. Mattheus, A. B. Dros, J. Baas, G. T. Oostergetel, A. Meetsma, J. L. de Boer, and T. T. M. Palstra, *Synth. Met.* **138**, 475 (2003).
- <sup>17</sup>T. Aoki-Matsumoto, K. Furuta, T. Yamada, H. Moriya, K. Mizuno, and A. H. Matsui, *Int. J. Mod. Phys. B* **15**, 3753 (2001).
- <sup>18</sup>C. D. Dimitrakopoulos, A. R. Brown, and A. Pomp, *J. Appl. Phys.* **80**, 2501 (1996).
- <sup>19</sup>T. Siegrist, C. Kloc, J. H. Schön, B. Batlogg, R. C. Haddon, S. Berg, and G. A. Thomas, *Angew. Chem., Int. Ed. Engl.* **40**, 1732 (2001).